Water Supply

Water Supply Vol 22 No 12, 8603 doi: 10.2166/ws.2022.391

Investigation of precipitation and extreme indices spatiotemporal variability in Seyhan Basin, Turkey

Cihangir Koycegiz and Meral Buyukyildiz *

Department of Civil Engineering, Konya Technical University, Konya, Turkey
*Corresponding author. E-mail: mbuyukyildiz@ktun.edu.tr

MB, 0000-0003-1426-3314

ABSTRACT

Spatial and temporal variability of precipitation increases with the effect of climate change. In this study, the Seyhan Basin has been determined as the study area. It is aimed to examine the spatiotemporal variability of precipitation and extreme precipitation indices in the Seyhan Basin. For this purpose, the period 1970–2019 was divided into three periods with the change point detection methods (Pettitt, Buishand rank and standard normal homogeneity test). Trends were examined by applying modified Mann–Kendall and Spearman's rho tests to precipitation and extreme indices for all periods and sub-periods. Then, temporal and spatial analyses of extreme indices were performed. According to the results obtained, there is no precipitation homogeneity throughout the basin. While the threat of drought comes to the fore with the decrease in rainy days and precipitation in the north, the risk of flooding is effective with the increase in precipitation intensity in the south.

Key words: change point detection, extreme indices, precipitation variability, Seyhan Basin, spatiotemporal analysis, trend

HIGHLIGHTS

- The spatiotemporal variability of precipitation and extreme precipitation indices in the Seyhan Basin was investigated.
- The change dates with change point detection methods were determined at the basin scale.
- The precipitation and extreme precipitation indices were analyzed with the modified Mann–Kendall and Spearman's rho trend tests.
- The results of analysis were mapped and interpreted.

GRAPHICAL ABSTRACT

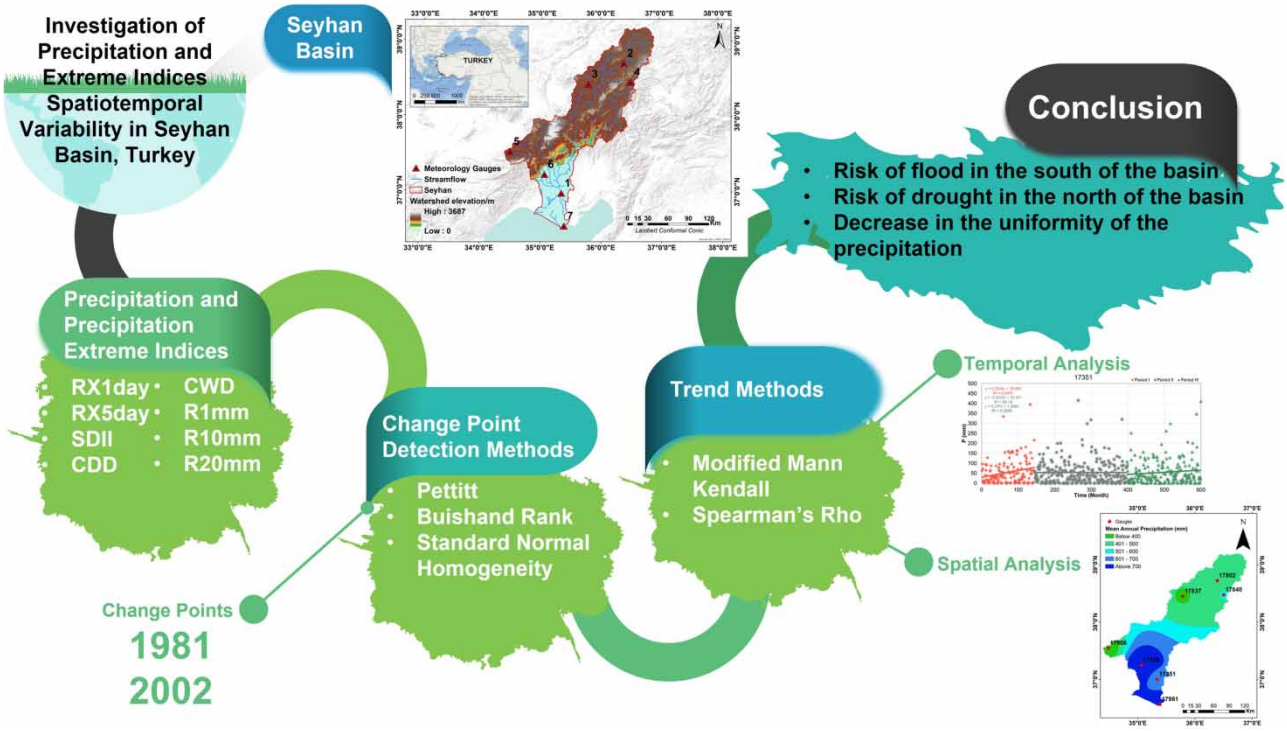

1. INTRODUCTION

Precipitation is one of the meteorological events most affected by climate change. Human intervention in water resources and land cover is also increasing with the rising population. This situation causes significant temporal and spatial changes in precipitation (Rysman *et al.* 2013). The spatial variation of precipitation leads to flood and drought problems in some regions. It also has a significant impact on the economies of countries. The temporal variability of precipitation negatively affects many sectors, especially agriculture. Investigating precipitation on a spatial and temporal scale is vital for the development of sustainable management strategies (van der Pol *et al.* 2015; Barbosa & Lakshmi Kumar 2016; Mehta & Yadav 2021). The variability of precipitation negatively affects not only eco-hydrological processes but also people's socio-economic lives (IPCC 2021).

Climate change causes severe droughts and extreme natural events around the world. The increasing irregularity of precipitation on a temporal and spatial scale hinders the efficient operation of basin-based planning. Since precipitation variability is very high in arid and semi-arid climatic regions, drought events in these climatic regions may cause greater ecological/economic losses.

It is necessary to observe and evaluate the variability of precipitation to take precautions against disasters and to use precipitation efficiently. At this point, extreme precipitation indices, which are frequently used in determining the characteristics of precipitation, come to the fore (Sillmann *et al.* 2013; Gao & Shi 2016; Jiang *et al.* 2016; Khedhaouiria *et al.* 2020; Saddique *et al.* 2020). Because of there usefulness, extreme precipitation indices are frequently preferred in hydro-meteorological studies (Zhang *et al.* 2011; Tongal 2019; Bhatti *et al.* 2020; Shawul & Chakma 2020). These indices assist in the effective analysis of large-scale precipitation data. In addition, the indices provide very useful information about the trend, variability and other statistical properties of precipitation (Alexander *et al.* 2019).

Statistical methods are frequently used to determine the characteristics of hydro-meteorological events. Trend analysis is widely used in studies such as the determination of short- or long-term changes among these methods. Non-parametric trend methods such as modified Mann–Kendall (MMK), Mann–Kendall (MK), Spearman's rho (SR), and Sen's T are frequently used in the analysis of hydrological phenomena (Tosunoğlu 2017; Pour *et al.* 2020; Zhai *et al.* 2020; Elzopy

et al. 2021; Esmaeilpour *et al.* 2021; Oscar-Júnior 2021). In addition, these methods are a powerful and effective tool in studies examining the variability in hydrological events.

Change point detection is very important in spatial and temporal variability analyses in hydrology (Tongal 2019). With change point detection, it is possible to examine periods with different behaviors that occur over time. Thus, current trends can be clearly examined. In the literature, there are many studies on change point analysis (Pettitt, standard normal homogeneity test, buishand range test, von neumann ratio test etc.) (Jaiswal *et al.* 2015; Abiy *et al.* 2019; Boluwade 2020; Ryberg *et al.* 2020).

Bhatti *et al.* (2020) analyzed the spatial and temporal changes in extreme precipitation indices in Pakistan using different statistical approaches (MK, sequential MK, Sen's slope estimator, Student's *T*-test, linear regression). As a result of the analysis, an increase in the spatial distribution of extreme precipitation indices was obtained as a whole. On the other hand, it was determined that extreme precipitation indices tended to decrease in humid regions affected by monsoon and westerlies during the study period. Mehta & Yadav (2021) investigated the trend of rainfall in the northwest region of India with the MK method, and the magnitude of the trends with the Sen's slope estimator. For the 102-year study period (1901–2002), an increasing trend was determined at $\alpha = 0.05$ significance level in annual, post-monsoon, pre-monsoon and southwest monsoon rainfall, while a decreasing trend was obtained in winter precipitation. Pour *et al.* (2020), using MMK, robust ITA, Sobol's method and sequential MK, investigated the changes in the reference evapotranspiration (ET_o) data of ten meteorological stations in peninsular Malaysia and the data of six meteorological parameters affecting it. Abiy *et al.* (2019) analyzed rainfall trends in southeast Florida with linear regression and MK tests, and the presence of a sudden rainfall change with the Pettitt test. Ros *et al.* (2016) examined the short- and long-term trends of rainfall data for the 1948–2011 period obtained from 50 stations in the Kelantan River Basin in the northeast Malaysian Peninsula with the MK test. In addition, the homogeneity of rainfall time series was investigated by using four absolute homogeneity tests, namely the Buishand range test, standard normal homogeneity test, Pettitt test and von Neumann ratio test.

The Seyhan Basin, which is used as the study area, is located in the south of Turkey. In addition to agricultural activities, industry also plays an important role in the socio-economics of the basin. A large part of the water used in the basin is allocated to drinking and utility water. In addition, irrigation water is allocated from the Seyhan Basin to the irrigation areas outside the basin (General Directorate of Water Management 2017). In the literature, there are studies indicating that the Seyhan Basin is under threat of drought (Topçu & Seçkin 2016; Tuncok 2016; Gumus & Algin 2017; Cavus & Aksoy 2019; Keskiner *et al.* 2019; Altın *et al.* 2020). In addition, significant decreasing trends in precipitation, snow water equivalent and flow have been determined in the Seyhan Basin (Gokmen 2016). Keskiner *et al.* (2019) examined the meteorological drought in the Seyhan Basin with the Standardized Precipitation Index (SPI) and Percent of Normal Index (PM) drought indices using monthly and annual rainfall data for the 1950–2006 period. Altın *et al.* (2020) conducted a hydrological drought analysis with the Streamflow Drought Index (SDI) in three-, six-, nine- and 12-month periods using monthly streamflow data of eight stations in the Seyhan and Ceyhan Basins. In another study, spatial drought was examined by calculating SPI on a 12-month time-scale using the data of 19 meteorology stations in the Seyhan Basin, and it was determined that different severities of drought were experienced in the basin (Cavus & Aksoy 2019).

The Seyhan Basin is the second largest basin after the Nile among the basins in the Eastern Mediterranean Basin. The Seyhan Basin, which has the most fertile lands in Turkey and Europe, is one of the richest regions in the world in terms of biodiversity, and dry and irrigated agriculture is practiced in most of the basin (Talu & Özüt 2011). The hydrology of the Seyhan Basin is also of great importance for the surrounding basins, as there is water allocation from the Seyhan Basin to the neighboring basins (Kızılırmak Basin and Ceyhan Basin) (General Directorate of Water Management 2017). According to the IPCC (2021), the Mediterranean Basin, where the Seyhan Basin is located, is among the basins that will be most affected by climate change. The spatial and temporal variability of precipitation due to climate change will significantly affect the socio-economic structure and biodiversity of the basin and will cause floods and droughts in the basin.

According to the literature review, as far as we know, it has been determined that there is no study on the Seyhan Basin that comprehensively examines the spatiotemporal variability of precipitation and extreme precipitation indices. Therefore, a comprehensive statistical study examining precipitation is very important for the basin.

The novelty of this study, in addition to the ones mentioned above, lies in the determination of a change point at the basin scale. The change point detection methods used within the scope of the study are generally preferred in the literature for the examination of a station or time series. However, in this study, it is aimed to determine a hydrological change point at the basin scale based on these methods. Thus, it is aimed to provide an up-to-date perspective on the use of single change

point determination methods in the literature. In addition, it is thought that examining the hydrological characteristics of the determined sub-periods will add scientific depth to hydrological time series analyses at the point of obtaining information that cannot be obtained from monotonic time series analyses. With such a perspective, it is thought that the investigation of precipitation and extreme precipitation indices for the study area will make important contributions to the science of hydrology in understanding the complex physics of precipitation.

The aim of this study is to determine the change points at the basin scale with change point detection methods, to analyze the precipitation and extreme precipitation indices with the modified Mann–Kendall and Spearman's rho trend tests, and to map and interpret the results. In summary, it is aimed to make a comprehensive statistical analysis of precipitation and extreme precipitation indices in the Seyhan Basin. It is thought that the results obtained may have utility for local administrators and policy makers in developing effective water-use strategies against climate change for the Seyhan Basin.

2. STUDY AREA AND DATA

Seyhan Basin, located in the south of Turkey, is located between 36° 30′ and 39° 15′ north latitudes and 34° 45′ and 37° 00′ east longitudes (Figure 1). The basin is adjacent to the Kızılırmak, Konya, and Eastern Mediterranean to the west, and Ceyhan and Euphrates Basins to the east. The Seyhan River in the Seyhan Basin is one of Turkey's most important rivers flowing into the Mediterranean. The drainage area of the Seyhan Basin is 22,035 km² and it constitutes approximately 2.82% of Turkey's surface area. The Seyhan River precipitation area is located in the Mediterranean and Central Anatolia geographical regions. Mediterranean climate is observed in the part of the basin in the Mediterranean region (the lower part), and terrestrial climate characteristics are encountered in the part in the Central Anatolia region (the middle and upper parts). In the Mediterranean climate, winters are warm and rainy, and summers are hot and dry. In the terrestrial climate, the winters are cold and usually snowy, and the summers are hot and dry.

In this study, daily precipitation data from seven meteorology stations in the Seyhan Basin during 1970–2019 were used. Some information regarding the daily precipitation statistics of the stations used is given in Table 1. According to Table 1, the

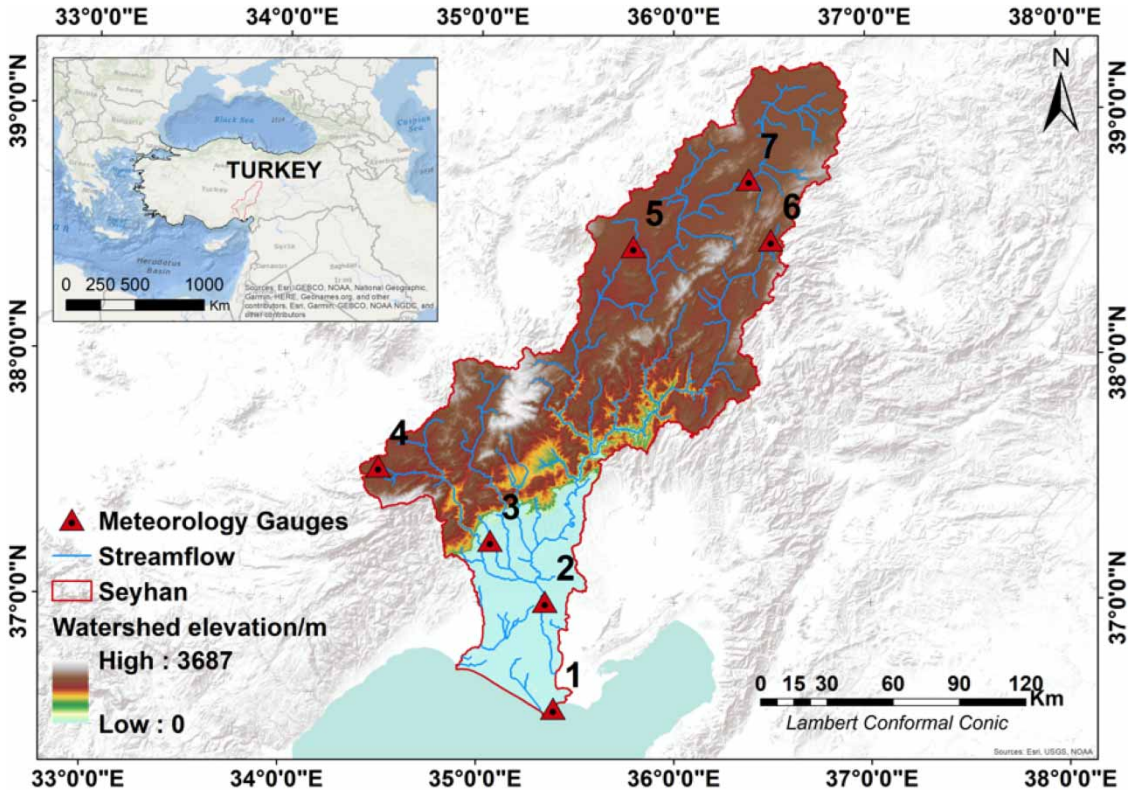

Figure 1 | The location of the Seyhan Basin in Turkey and the location on the Seyhan Basin of the seven meteorology gauge stations used in this study.

Table 1 | Descriptive statistics of daily precipitation data of seven meteorology measurement stations in the Seyhan Basin for the period 1970–2019

	Station number	Station name	Elevation (m)	Min (mm)	Max (mm)	Mean (mm)	Standard deviation (mm)	Skewness
1	17981	Karataş	22	0	199.4	2.108	8.184	7.327
2	17351	Adana	23	0	147	1.785	6.963	7.430
3	17936	Karaisalı	240	0	231	2.397	8.711	7.057
4	17906	Ulukışla	1,453	0	60	0.877	2.981	6.253
5	17837	Tomarza	1,402	0	46.1	1.064	3.244	5.110
6	17840	Sarız	1,599	0	76,9	1.387	3.928	5.174
7	17802	Kayseri/Pınarbaşı	1,542	0	49.9	1.116	3.210	4.871

station with the lowest daily mean precipitation is Ulukışla at 0.877 mm, and the station with the highest is Karaisalı (No:17936) at 2.397 mm. The stations with the lowest and highest daily maximum precipitation are Tomarza (No:17837) and Karaisalı (No:17936) stations at 46.1 and 231 mm values, respectively. The lowest and highest standard deviation values are obtained at Ulukışla (No:17906) and Karaisalı (No:17936) stations with the values of 2.981 and 8.711, respectively. Kayseri/Pınarbaşı station has the lowest skewness value at 4.871, while Adana station (No:17351) has the highest skewness value at 7.430. It is observed that there is a decrease in the amount of precipitation in general from the south to the north of the basin (Table 1).

3. METHODOLOGY

3.1. Change point detection methods

It is very important to determine the change point in the analysis of time series. The presence of a change point indicates a sudden and significant change in the data generation process. In this study, three methods, namely the Pettitt test (PT) (Pettitt 1979), Buishand rank test (BRT) (Buishand 1982) and standard normal homogeneity test (SNHT) (Alexandersson 1986), were used for change point detection. These three tests are capable of identifying the year in which a break is likely in a time series. SNHT has a characteristic feature in detecting breaks near the beginning and the end of a time series (Wijngaard *et al.* 2003). In the non-parametric PT, the corresponding order of the data is taken into account instead of the value. The sequencing approach makes the PT less sensitive than the other tests. Unlike SNHT, PT and BRT are more sensitive to detecting breaks in the middle of time series. SNHT and BRT assume that the data are normally distributed, while PT does not require this assumption. In these three methods, the null hypothesis (H_0) indicates that the series has independent and random distribution, while the alternative hypothesis (H_1) indicates that there is a sudden change. The mathematical formulation of SNHT, BRT and PT and their critical values for test statistics are not given here because they are available in many studies in the literature (Pettitt 1979; Buishand 1982; Alexandersson 1986; Ros *et al.* 2016).

3.2. Trend detection methods

3.2.1. Modified Mann–Kendall test

One of the important points in trend analysis studies is the serial correlation within the time series, that is, autocorrelation. The presence of autocorrelation in a time series causes the rejection of the null hypothesis that there is no trend in the series and the detection of trends that do not exist when there is no real trend in the series (Chen *et al.* 2016). The modified Mann–Kendall (MMK) test was proposed by Hamed & Rao (1998) to eliminate the autocorrelation problems in the classical Mann–Kendall trend test. In this test, a variance correction approach is used to improve the trend analysis. The Mann–Kendall statistic (S) for the x_1, x_2, x_3… and x_n time series is calculated as follows:

$$S = \sum_{k=1}^{n-1} \sum_{j=k+1}^{n} \operatorname{sgn}(x_j - x_k) \tag{1}$$

$$\operatorname{sgn}(x_j - x_k) = \begin{cases} +1 & \text{if} \quad (x_j - x_k) \\ 0 & \text{if} \quad (x_j - x_k) \\ -1 & \text{if} \quad (x_j - x_k) \end{cases} \tag{2}$$

The variance of the S statistic (Var(S)) and the adjusted variance (Var*(S)) are calculated with Equations (3) and (4), respectively:

$$\mathrm{Var}(S) = n(n-1)(2n+5)/18 \tag{3}$$

$$\mathrm{Var}^*(S) = \mathrm{Var}(S) x \frac{n}{n_s^*} \tag{4}$$

In Equation (4), n/n_s* is the autocorrelation correction factor and is calculated by Equation (5):

$$\frac{n}{n_s^*} = 1 + \frac{2}{n(n-1)(n-2)} \sum_{i=1}^{n-1} (n-i)(n-i-1)(n-i-2)\rho_{(i)} \tag{5}$$

where n is the number of observations in the time series, and $\rho_{(i)}$ is the autocorrelation function of the ranks (i) of the time series. The standardized Z value is calculated by Equation (6). The significance of the trend is determined by comparing the standardized Z value with the Z_{critical} at α significance level.

$$Z = \left\{ \begin{array}{lll} \dfrac{S-1}{\sqrt{\mathrm{Var}^*(S)}} & \text{if} & S > 0 \\ 0 & \text{if} & S = 0 \\ \dfrac{S+1}{\sqrt{\mathrm{Var}^*(S)}} & \text{if} & S < 0 \end{array} \right\} \tag{6}$$

If $|Z|$ is larger than $Z_{1-\alpha/2}$, then the null hypothesis (H_0) is rejected and so, H_1 is accepted. In this test, H_0 represents no-trend while H_1 indicates that the time series has meaningful increasing or decreasing trends. If the Z value is negative (positive), there is a decreasing (an increasing) trend.

3.2.2. Spearman's rho test

Spearman's rho (SR) test is a quick and simple test for investigating the existence of a linear trend, based on rank statistics. The rank statistic $R(x_i)$ is determined by ordering the observations from smallest to largest or from largest to smallest. The SR test value (r_s) is calculated by Equation (7), where i is the order of observation of the data and n is the number of observations, and the test statistic z is calculated by Equation (8):

$$r_s = 1 - 6\frac{\left[\sum_{i=1}^{n} (R(x_i) - i)^2\right]}{(n^3 - n)} \tag{7}$$

$$z = r_s\sqrt{n-1} \tag{8}$$

If the $|z|$ value is greater than the z_α value ($|z| > z_\alpha$) determined from the standard normal distribution table at the chosen significance level α, the H_0 hypothesis, which is based on the fact that the observation values do not change over time, is rejected and it is concluded that there is a certain trend (Lehman & D'Abrera 1975; Sneyers 1990).

3.3. Extreme precipitation indices

The Expert Team on Climate Change Detection (ETCCD) defined 27 extreme climate indices to analyze the observed or modeled precipitation and temperature parameters. Eleven of these indices are related to precipitation parameters and eight of these indices (RX1day, RX5day, SDII, CDD, CWD, R1mm, R10mm and R20mm) were examined within the scope of this study (Table 2). RX1day, RX5day and SDII are used to determine extreme precipitation events, while CDD and CWD are used to examine the seasonality of precipitation (Tao *et al.* 2018). Threshold indices R1mm, R10mm and R20mm are also used to categorize precipitation days (Sillmann *et al.* 2013). Thus, in addition to the extreme precipitation days, information can be obtained about the number of heavy precipitation and wet days. The indices used were calculated manually in Excel on an annual scale. The descriptions and formulas for each index are found in Zhang *et al.* (2011).

Table 2 | Definition of the precipitation indices used in this study

Indices	Indicator name	Description	Unit
RX1day	Maximum one-day precipitation	Annual highest daily precipitation	mm
RX5day	Maximum five-day precipitation	Annual maximum consecutive five-day precipitation	mm
SDII	Simple precipitation intensity index	The daily precipitation amount on wet days	mm/day
CDD	Number of consecutive dry days	Maximum number of consecutive dry days with RR < 1 mm	day
CWD	Number of consecutive wet days	Maximum number of consecutive wet days with RR ≥ 1 mm	day
R1mm	Number of wet days	Annual count of days when PRCP ≥ 1 mm	day
R10mm	Heavy precipitation days	Annual count of days when PRCP ≥ 10 mm	day
R20mm	Very heavy precipitation days	Annual count of days when PRCP ≥ 20 mm	day

Note: RR is the daily precipitation.

4. RESULTS AND DISCUSSION

4.1. Determination of change points and sub-periods

Within the scope of the study, three different methods were used (PT, BRT, SNHT) to obtain reliable results in the determination of the change point. The application of a single method in the detection of the change point may cause inaccuracies in the detection of the change point (Tao *et al.* 2018). In station-based change point determination studies, it is not possible to examine behavior at the basin scale. In the examined period, the years in which the change was determined in seven stations according to all three methods were taken into account and the results are given in Table 3.

The values in Table 3 represent the number of statistical methods in which the change is determined in the relevant station and year. For the period 1970–2019, there is no change point in all three statistical methods in the years not given in Table 3. For example, the year 1973 was obtained as the change point in two and one statistical methods at stations 17351 and 17981, respectively. However, there is no change in other stations for this year. At stations 17802, 17906 and 17936, the year 1981 was obtained as the change point in three, one and one statistical methods, respectively. Similarly, the year 2002 was obtained as the change point in one, two and one statistical methods, respectively, at stations 17840, 17936 and 17981. As a result of the evaluation made in this way, the years with the highest change were determined as 1981 and 2002. In line with the results obtained, the period 1970–2019 was divided into three sub-periods: first period 01.01.1970–31.12.1981; second period 01.01.1982–31.12.2002; third period 01.01.2003–31.12.2019.

4.2. Spatiotemporal analysis of monthly precipitation for sub-periods

To evaluate the general behavior of the monthly precipitation data of the seven stations used in the three sub-periods, the time series were drawn and linear trends of the sub-periods were determined (Figure 2). In addition, the monthly mean precipitation data of the three sub-periods for each station is given in Figure 3. From the graphs in Figures 2 and 3, it is seen that the sub-periods behave differently in some stations. For example, in 17351, there is an increasing (0.332 mm/month),

Table 3 | Results of statistical tests that defined a change point for seven stations in the Seyhan Basin

Station number	1973	1974	1981	1994	1997	1998	2002	2010	2012
17351	2	0	0	0	1	0	0	0	0
17802	0	0	3[a]	0	0	0	0	0	0
17837	0	0	0	0	0	0	0	1	2
17840	0	0	0	0	0	1	1	1	0
17906	0	0	1	2	0	0	0	0	0
17936	0	0	1	0	0	0	2	0	0
17981	1	1	0	0	0	0	1	0	0

[a]For example, three statistical tests at station 17802 revealed that it was the change point for 1981. The years (1981 and 2002) to which the shaded values belong represent the change point years.

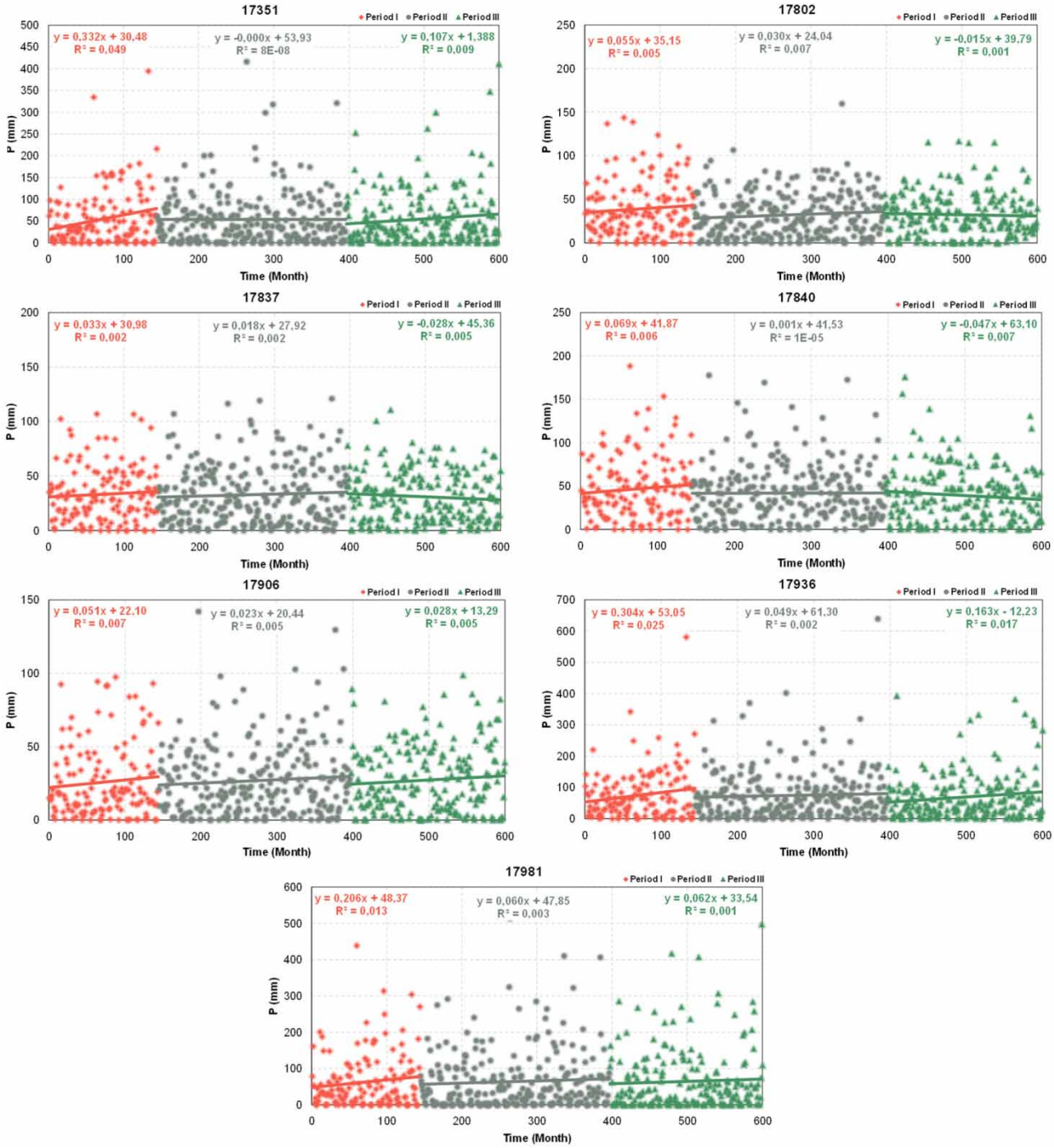

Figure 2 | Linear trends of monthly precipitation of the seven stations for the three sub-periods.

decreasing (−0.000 mm/month) and increasing (0.107 mm/month) trend in the sub-periods, respectively. At stations 17802, 17837, and 17840, there is an increasing trend in Period 1 and Period 2, and a decreasing trend in Period 3. In other stations, there is an increasing trend in monthly precipitation data in each sub-period. For Period 1 (1970–1981), the highest increasing trend is observed at stations 17351 (0.332 mm/month), 17936 (0.304 mm/month) and 17981 (0.206 mm/month) in the south of the basin. In Period 2, there is generally a fairly small uptrend at all stations (a very small downtrend at 17351). In Period 3 (2003–2019), there is a slightly decreasing trend at stations 17802, 17837 and 17840, while there is an increasing trend at the

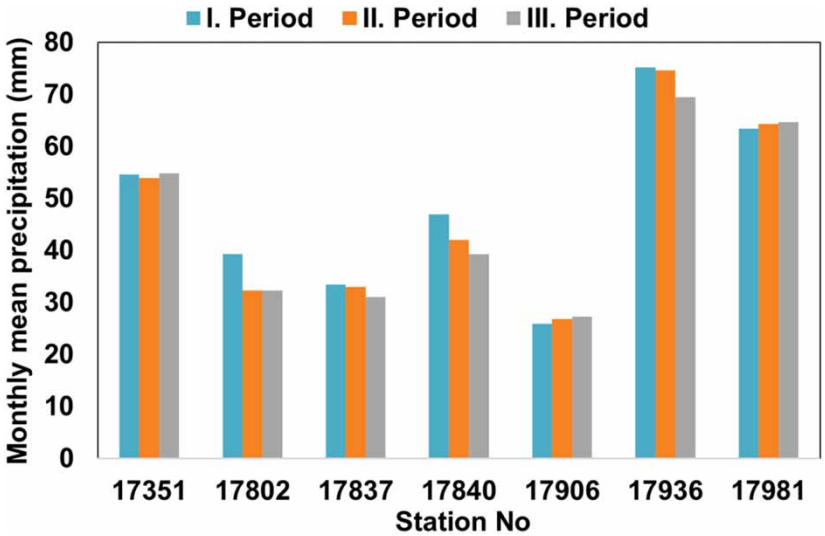

Figure 3 | Mean of monthly precipitation data for the three sub-periods.

other stations. In this period, the station with the highest decreasing trend in monthly precipitation is 17840 (0.047 mm/month), while the station with the highest increasing trend is 17936 (0.163 mm/month).

According to Figure 3, the stations with the highest monthly mean precipitation for all three sub-periods are 17936, 17981 and 17351 (south of the basin), and the stations with the lowest are 17906 (west of the basin), 17837, 17840, 17802 (north of the basin) (Figure 1). It is thought that this difference in the monthly mean precipitation data of the stations is due to the terrestrial climate in the north and west of the basin and the Mediterranean climate in the south. If an evaluation is made for the monthly mean precipitation data in terms of the change between all three periods, stations 17906 and 17981 generally show similar behavior to each other, and the other stations show similar behavior to each other. In five of the seven stations (except 17906 and 17981), there is a decrease in monthly mean precipitation from Period 1 to Period 2. The stations with the highest decrease are stations 17802 and 17840 (Figure 3).

In Figure 4, the spatially distributed map of the mean annual precipitations of the Seyhan Basin for the whole period and three sub-periods is given. It is seen in Figure 4(a) that in the whole data period, the highest precipitation in the basin is in the south of the basin at stations 17936 and 17981 (>700 mm/year) and the lowest precipitations are in the west and north of the basin, at stations 17906 and 17837 (<400 mm). When Figure 4(b)–4(d) is examined, it is seen that the spatial distribution of precipitation for each sub-period exhibits a behavior very similar to that in the entire period. The most significant change in the distribution of precipitation between sub-periods occurs in the north of the basin. The precipitation amount, which is 101–500 mm/year in 17837 and 17802 in Period 1, is <400 mm/year in Period 2 and Period 3. In Period 3, the area represented by >400 mm/year at these stations increases further. The area in the north of the basin, which is generally represented by 501–600 mm/year in Period 1, decreases a lot in Period 2 and completely disappears in Period 3. This indicates that there is a drought from Period 1 to Period 3 for the north of the basin. There is no significant change in the spatial distribution of precipitation at stations in the south of the basin according to sub-period.

4.3. The results of trend analysis for extreme precipitation indices

Trend analysis was performed at a 5% significance level by using non-parametric modified Mann–Kendall (MMK) and Spearman's rho (SR) tests in eight extreme precipitation indices applied to the daily precipitation data of the seven meteorology stations in the Seyhan Basin. Trend analysis was carried out both in the period 1970–2019 and in the three sub-periods determined as a result of the change point analysis. The trend analysis results for the 1970–2019 period are given in Table 4, and the trend analysis results for the three sub-periods are given in Figure 5.

The SR and MMK trend analysis results given in Table 4 for the period 1970–2019 are quite close to each other. According to the trend analysis results obtained, there is a generally insignificant decreasing trend in most of the precipitation indices at the stations in the north of the basin (17802, 17837, 17840) compared with both SR and MMK methods. A significant

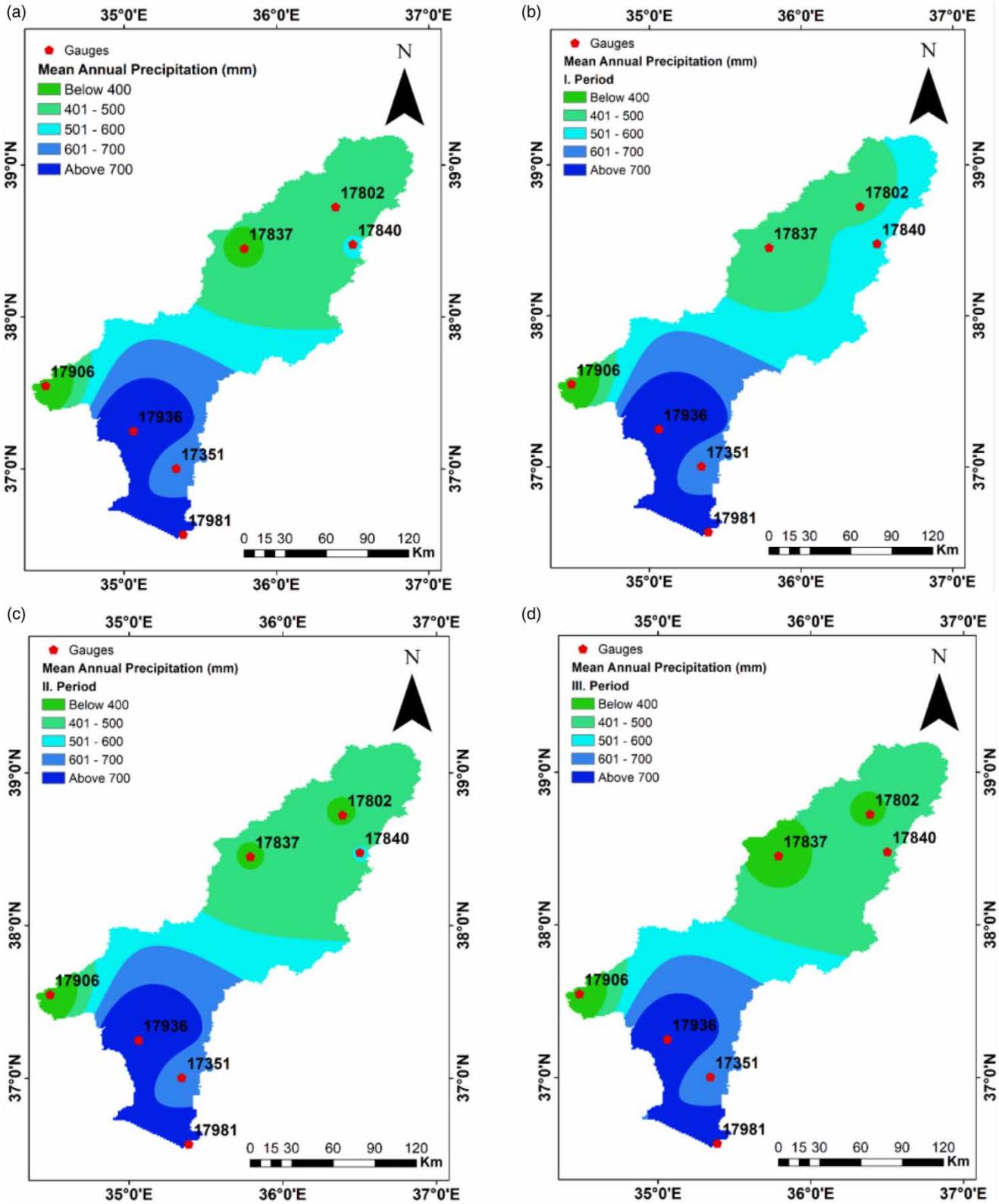

Figure 4 | Spatial distribution of mean annual precipitation for (a) the whole period (1970–2019) and sub-periods: (b) Period 1 (1970–1981), (c) Period 2 (1982–2002) and (d) Period 3 (2003–2019).

Table 4 | Trend analysis results of extreme precipitation indices for the whole period (1970–2019)

	Stations													
	17351		17802		17837		17840		17906		17936		17981	
Indices	SR	MMK	SR	MMK	SR	MMK	SR	MMK	SR	MMK	SR	MMK	SR	MMK
RX1	0.52	0.47	−0.69	−0.72	−0.36	−0.34	−0.94	−0.96	**2.26****	**2.33****	−0.2	−0.17	0.17	0.11
RX5	0.34	0.34	−0.8	−0.8	−0.6	−0.64	−1.4	−1.42	**2.24****	**2.28****	−0.34	−0.33	−0.12	−0.14
CDD	−0.68	−0.72	0.26	0.16	−1.25	−1.5	0	0	0.89	0.84	−1.66	−1.58	−0.01	−0.05
CWD	−0.24	−0.38	−0.18	−0.35	−0.55	−0.8	−0.92	−1.07	0.42	0.08	−0.59	−0.76	1.22	1.08
SDII	1.33	1.3	−1.74	−1.73	**−2.15***	**−2.11***	**−3***	**−2.93***	**2.14****	**2.23****	0.61	0.62	0.22	0.14
R1	0.17	0.36	−1.79	−1.78	0.1	0.13	**−3.83***	**−3.87***	−0.36	−0.2	−0.1	0.03	−0.84	−0.88
R10	0.17	0.04	−1.52	−1.56	−0.5	−0.67	−0.71	−0.69	1.63	1.75	−0.03	−0.11	−0.11	−0.25
R20	1.42	1.42	−0.44	−0.59	0.22	0.15	**−2.21***	**−2.37***	**2.7****	**2.43****	0.3	0.24	0.4	0.32

**Significant positive trend at 5% level.
*Significant negative trend at 5% level.

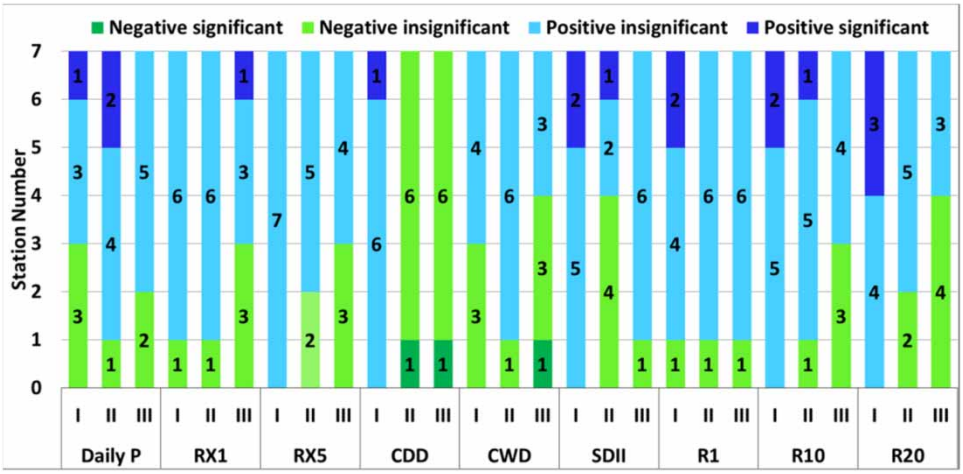

Figure 5 | Trends of the precipitation indices expressed as the number of stations.

decreasing trend is obtained in SDII at station 17837 and SDII, R1mm and R20mm indices at station 17840. Increasing trends in precipitation indices are generally determined at station 17906 located in the west of the Seyhan Basin and at stations 17351 and 17981 in the south, and most of them are insignificant increasing trends. There is an insignificant decreasing trend in the CDD and CWD indices at station 17351, and an insignificant increasing trend in the other indices. Significant uptrends are found only in the indices of RX1day, RX5day, SDII and R20mm at station 17906 in the west of the basin. In this station, there is an insignificant decreasing trend in the R1mm index, while an insignificant increasing trend is found in the other indices. According to Table 4, the RX1day, RX5day and R10mm indices generally show similar behavior in the 1970–2019 period. An insignificant decreasing trend is determined at the 0.05 significance level at four stations in the RX1day index and five stations in the RX5day and R10mm indices. The index with the highest increasing trend is R20mm, and there is a decreasing trend in this index only at stations 17802 (insignificant) and 17840 (significant) in the north of the basin, and there is an increasing trend at the other stations.

The results obtained for the three sub-periods examined according to the SR and MMK trend analyses are given in Table 5, and the results based on the number of stations depending on the trend status are given in Figure 5. According to the trend analysis results of the three sub-periods, there is a mostly insignificant increasing trend (62%) in all periods and indices (Table 5 and Figure 5). Also, a 1.5% significant decreasing trend, 28% insignificant decreasing trend and 8.5% significant increasing trend were obtained (Figure 5). Only in the CDD index, a decreasing trend is determined in the seven stations

Table 5 | Trend analysis results of extreme precipitation indices for the three sub-periods

		Stations													
		17351		17802		17837		17840		17906		17936		17981	
Indices	Period	SR	MMK	SR	MMK	SR	MMK	SR	MMK	SR	MMK	SR	MMK	SR	MMK
Daily P	I	**2.00****	**2.04****	−1.60	−1.63	−1.40	−1.42	−0.52	−0.57	0.75	0.78	1.20	1.25	1.65	1.68
	II	0.05	0.07	**4.00****	**4.17****	**2.94****	**2.97****	1.15	1.17	−1.01	−1.05	0.15	0.17	0.86	0.91
	III	0.70	0.75	0.04	0.07	−1.11	−1.15	−1.90	−1.94	1.15	1.19	1.65	1.70	0.90	0.95
RX1	I	1.78	1.80	1.49	1.51	1.57	1.62	0.92	0.93	0.51	0.60	0.14	0.16	−0.09	−0.04
	II	−1.13	−1.18	1.01	1.01	0.03	0.01	0.11	0.04	1.89	1.86	0.60	0.69	1.38	1.28
	III	0.91	0.93	−0.76	−0.75	−0.98	−0.93	−0.65	−0.73	1.03	1.08	**2.12****	**2.23****	0.76	0.72
RX5	I	1.77	1.85	1.36	1.36	1.63	1.57	1.09	1.08	0.82	0.90	0.63	0.70	0.44	0.45
	II	−0.84	−0.83	1.14	1.13	0.44	0.36	−0.29	−0.38	1.11	1.13	0.40	0.49	0.81	0.75
	III	0.83	0.83	−0.26	−0.21	−1.11	−1.06	−0.42	−0.46	1.33	1.37	1.12	1.16	0.35	0.28
CDD	I	1.37	1.44	1.53	1.58	0.86	0.89	1.34	1.23	1.77	1.78	2.46	2.67	1.14	1.03
	II	−0.27	−0.36	**−2.21***	**−2.48***	−0.04	−0.15	−1.86	−1.87	−0.46	−0.42	−0.87	−0.75	−1.44	−1.33
	III	−0.25	−0.16	−1.56	−1.36	**−2.30***	**−2.47***	−0.23	−0.25	−0.63	−0.74	−1.49	−1.48	−0.46	−0.45
CWD	I	1.25	1.10	−0.36	−0.48	−1.81	−1.65	0.13	0.00	−0.16	−0.14	0.51	0.27	0.26	0.07
	II	1.68	1.45	0.26	0.00	−0.36	−0.45	1.02	0.88	0.30	0.06	0.09	0.09	0.00	0.00
	III	−0.02	−0.04	0.23	0.16	**−2.08***	**−2.06***	0.23	0.21	−0.08	−0.37	−0.28	−0.29	0.07	0.04
SDII	I	1.93	1.95	**2.94****	**2.92****	1.65	1.64	**2.57****	**2.61****	0.30	0.32	0.56	0.71	0.11	0.05
	II	−0.54	−0.58	−0.26	−0.27	−1.73	−1.63	−0.13	−0.13	**2.56****	**2.54****	1.12	1.15	1.45	1.35
	III	0.47	0.43	−0.17	−0.11	0.51	0.46	0.03	0.07	0.49	0.47	1.00	1.04	0.63	0.52
R1	I	**2.66****	**2.88****	0.47	0.48	−0.52	−0.69	1.39	1.23	1.21	1.17	1.90	1.85	**2.62****	**2.67****
	II	1.16	1.18	1.40	1.30	0.66	0.85	0.33	0.39	−0.19	0.00	0.93	0.94	0.81	0.63
	III	1.07	1.07	0.04	0.00	0.45	0.29	−1.11	−0.95	1.03	1.11	1.32	1.32	0.19	0.00
R10	I	**2.41****	**2.26****	1.15	0.96	1.95	1.65	1.42	1.37	1.08	0.96	**2.41****	**2.33****	1.22	0.96
	II	−0.09	−0.06	1.54	1.27	0.61	0.54	0.49	0.42	**1.99****	**1.96****	1.69	1.57	0.77	0.42
	III	0.91	0.82	−0.36	−0.29	−1.14	−1.07	−0.66	−0.58	1.58	1.77	1.58	1.44	0.65	0.45
R20	I	1.90	1.82	**2.32****	**1.99****	**1.97****	**2.06****	0.99	0.75	1.93	1.78	**2.40****	**2.40****	1.94	1.78
	II	−0.64	−0.57	0.73	0.48	1.48	1.36	−1.25	−1.15	1.50	1.18	1.14	1.03	0.94	0.82
	III	0.48	0.58	−0.26	−0.37	−0.60	−0.66	−1.15	−1.28	0.88	0.66	1.22	1.07	−0.02	−0.04

**Significant positive trend at 5% level.
*Significant negative trend at 5% level.

examined in Period 2 and Period 3. RX5day, CDD, SDII, R10mm and R20mm indices show an increasing trend at all stations in Period 1. Significant decreasing trends are obtained in the CDD index (station 17802) in Period 2, and in the CDD and CWD indices (station 17837) in Period 3.

According to Figure 5, most of the significant uptrends are found in Period 1. There is no significant increasing trend in any of the stations and indices in Period 3. Significant or insignificant increasing trends are detected in R1mm and R10mm indices at all stations (Figure 5 and Table 5). Also, an increasing trend is determined in all indices and periods at stations 17936 and 17981. The highest decreasing trend is found at stations 17837 and 17840 located in the north of the basin (Table 5).

4.4. Temporal variability in precipitation

Box plots for the annual CDD and CWD indices of the stations for the whole period and the three sub-periods are given in Figure 6. In Figure 6(a), it is seen that there is a decrease in the median/min/max values of CDD from Period 1 to Period 2, and an increase from Period 2 to Period 3. Period 2 is the period with lower CDD values compared with the other periods, with min = 17 days, median = 57 days and max = 131 days. Period 3, on the other hand, has high min, median and max CDD values and is determined to be the driest period compared with the other sub-periods. Although there are outliers in maximum CDD values in all periods, it is seen that these outliers are higher in Period 3 (2003–2019) compared with the other periods. In the box plots of the CWD values in Figure 6(b), it is seen that the minimum CWD values of all periods and the median values of the whole period and the 2nd and 3rd sub-periods are quite close to each other. The CWD values are skewed positively in Period 3 and negatively in Period 2. On the other hand, it is seen that the CWD values for Period 2 are normally distributed throughout the basin.

According to the box plots given in Figure 7 for the RX1day and RX5day indices, the min and median values are rather close to each other in all four periods examined. When the highest RX1day and RX5day values are examined, Period 2

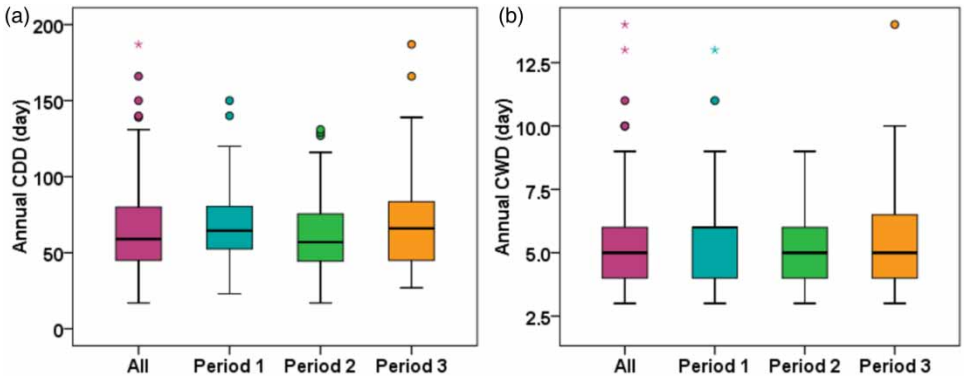

Figure 6 | Box plots for annual (a) CDD and (b) CWD.

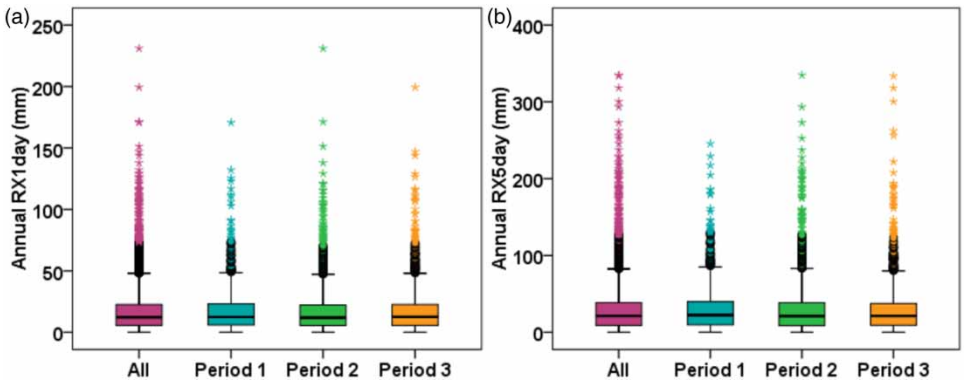

Figure 7 | Box plots for annual (a) RX1day and (b) RX5day.

has the highest and Period 1 has the lowest values. Period 2 and Period 3 show almost the same behavior in RX5day. Many outliers are observed in all periods in the RX1day and RX5day indices.

According to the box plots of the R1mm index (Figure 8), there is a decrease in the median and maximum values from the first period to the third period. There is a decrease in the minimum R1mm values from the first period to the second period, and an increase from the second period to the third period. In the R1mm index, Period 1 shows a skewed distribution in the positive direction and Period 3 in the negative direction. The R1mm index varies in the ranges of 46–105, 33–100 and 39–91 days in the examined sub-periods (from the first period to the third period, respectively). According to Figure 8, the R10mm index has the same number of days in all sub-periods in minimum values and the second and third periods in median values. The R10mm index values of the first and second periods show a positively skewed distribution. Period 2 and Period 3 have maximum outliers in the indices R1mm and R10mm, respectively. For the indices R1mm and R10mm, the median value in the whole period (1970–2019) has a lower value than in the other three sub-periods. In the box plots of the R20mm index (Figure 8), it is seen that the min, max and median values are almost the same in all three sub-periods and the R20mm index values of the three periods show a positively skewed distribution. The R20mm index for the whole period (1970–2019) shows very similar behavior to Period 1 and has positive skewness. According to the graphs of the R20mm index, there are no outliers in any period. R20mm values vary in the range 0–21 in the whole period and third period, and 0–20 in the first period and second period. The median values for the R20mm index are the same in all periods (four days). In the SDII index, the minimum and median values are almost the same in all periods, and the maximum SDII value is obtained in the third sub-period. In addition, there are many outlier SDII values in the whole period and three sub-periods (Figure 8).

4.5. Spatial variability in precipitation

The spatial distribution of eight extreme precipitation indices used to determine the effect of climate change on precipitation variability in the Seyhan Basin was investigated. The study was carried out for the whole period and three sub-periods. The

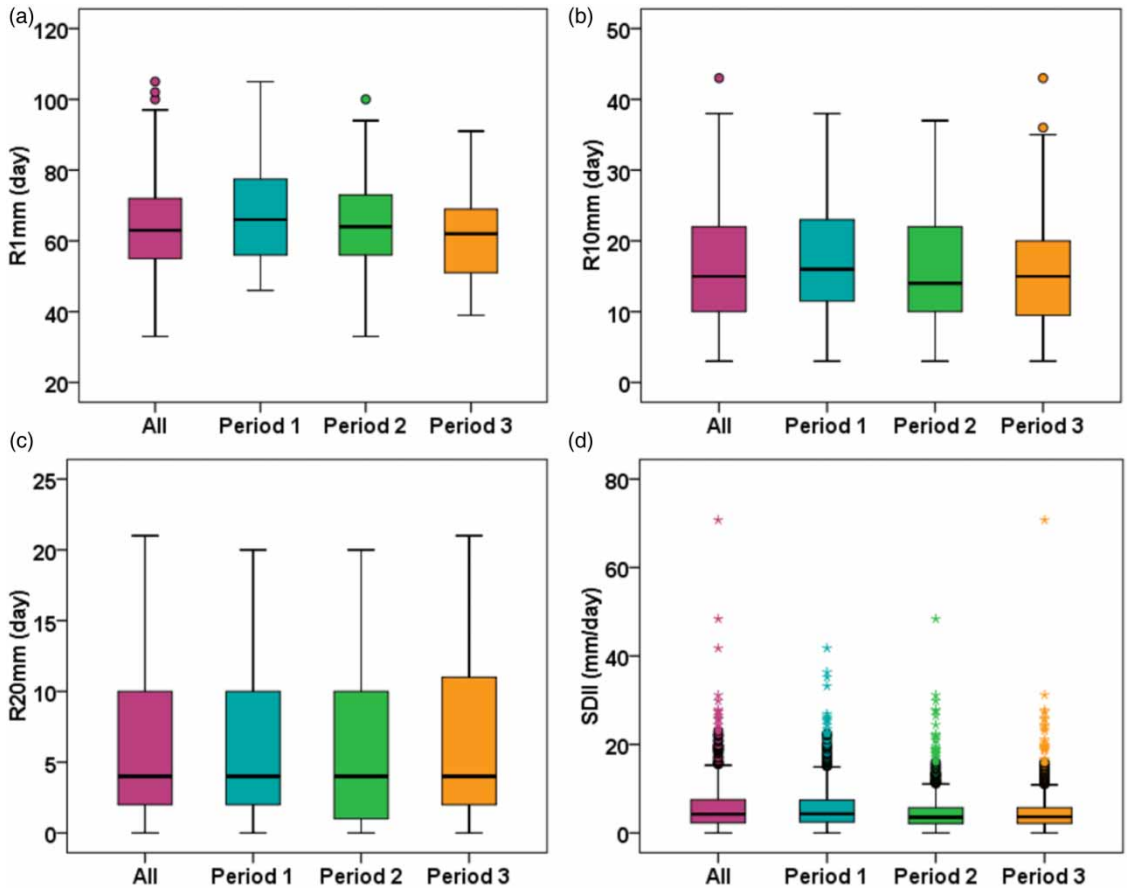

Figure 8 | Box plots for (a) R1mm, (b) R10mm, (c) R20mm and (d) SDII.

inverse distance weight (IDW) method, which is frequently used in the literature, is used to convert point data into spatial information (Fisher *et al.* 1987).

Consecutive dry days (CDD) index and consecutive wet days index (CWD) maps for the whole period (1970–2019) are given in Figure 9, and maps of the three sub-periods for both indices are given in Figure 10. According to Figure 9(a), the highest CDD value is obtained at station 17981. The fact that CDD values are high in the southern parts of the basin, where precipitation is high, indicates that short-term heavy precipitation has fallen in this region. Also, the fact that the southern regions of the basin are under the influence of the Mediterranean climate can be considered as the reason for this result. The lowest CDD values are determined in the north of the basin, and according to Figure 3(a), these regions are regions with low annual mean precipitation and terrestrial climate.

According to the maps given for the sub-periods (Figure 10(a)–10(c)), CDD values show a decrease from Period 1 to Period 2, and a general increase in CDD values is observed in Period 3 (in regions outside the south of the basin). This is clearly seen both in the box plot for CDD (Figure 6(a)) and in the trend results (Table 5). There is a general decrease in CDD values from Period 1 to Period 3 in the south of the basin. The high CDD values of the basin in the third period indicate agricultural droughts. The increase in precipitation intensity in the basin, where agriculture is intense, not only makes it difficult to control water resources, but also complicates agricultural planning strategies.

According to the CWD map given in Figure 9(b) for the whole period, CWD values vary between 4.56 and 6.52 days, the lowest CWD values are obtained at station 17906 and the highest CWD values are obtained at station 17981. According to Figure 10(d)–10(f), and when looking at the basin as a whole, there is a gradual decrease in general over the three periods. The eastern side of the basin has more consecutive precipitation days compared with the western side. CWD is crucial for maintaining soil moisture and flow dynamics in the watershed (Tongal 2019).

The spatial distribution of the indices of wet days (R1mm), heavy precipitation days (R10mm) and very heavy precipitation days (R20mm) for the period 1970–2019 is shown in Figure 11. While the low R1mm values are present in the southern parts of the basin, which is under the influence of the Mediterranean precipitation regime, the higher R1mm values are observed in the northern parts with terrestrial climate characteristics (Figure 11(a)). The highest R1mm for the entire period in the basin was obtained at station 17840. According to the spatial variability maps of the R10mm and R20mm indices (Figure 11(b) and

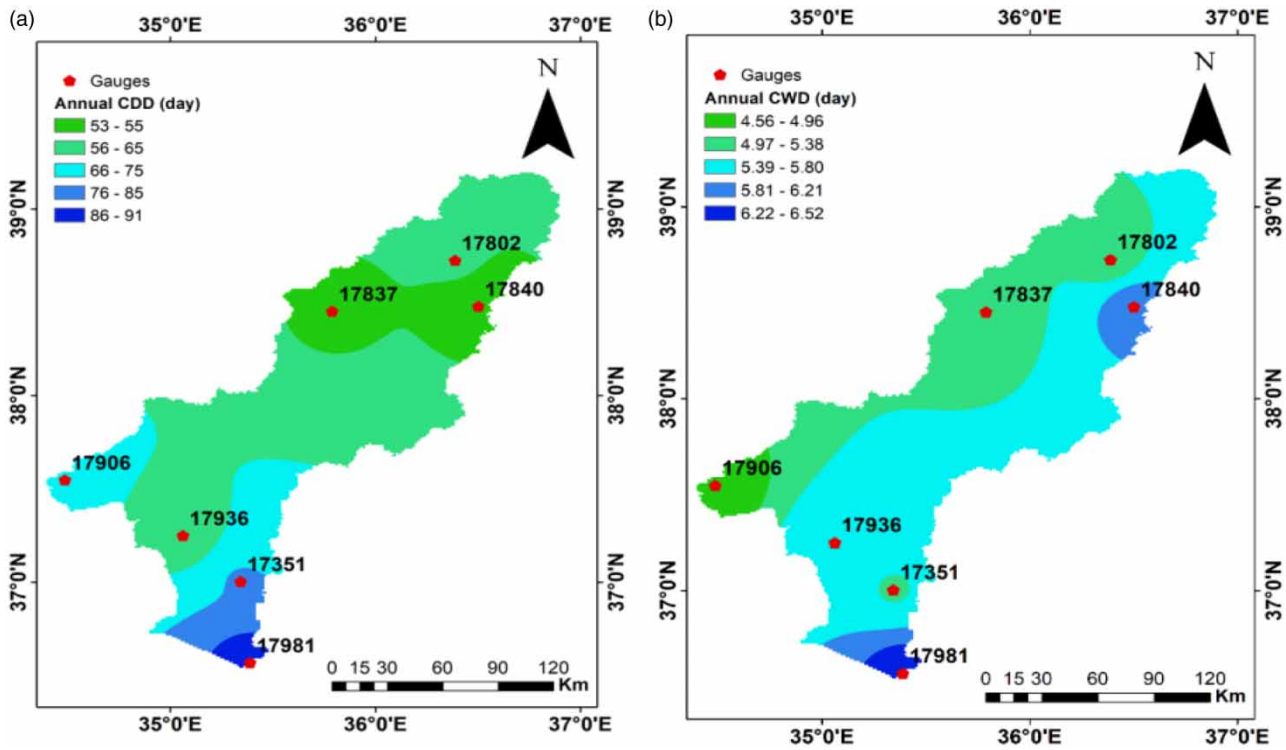

Figure 9 | Spatial variability of (a) CDD and (b) CWD for the whole period (1970–2019).

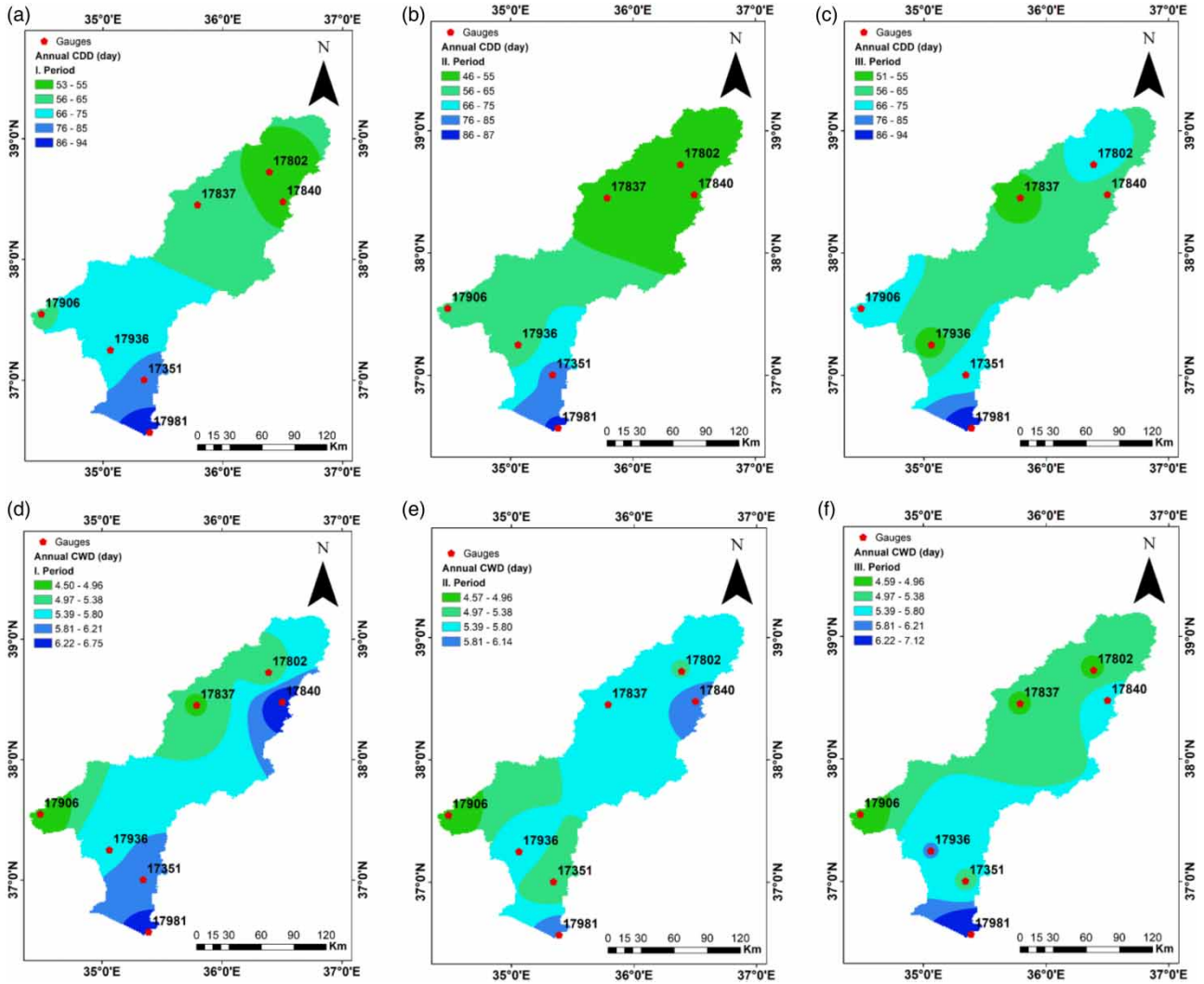

Figure 10 | Spatial variability of CDD and CWD for sub-periods: (a) CDD-Period 1, (b) CDD-Period 2, (c) CDD-Period 3, (d) CWD-Period 1, (e) CWD-Period 2, (f) CWD-Period 3.

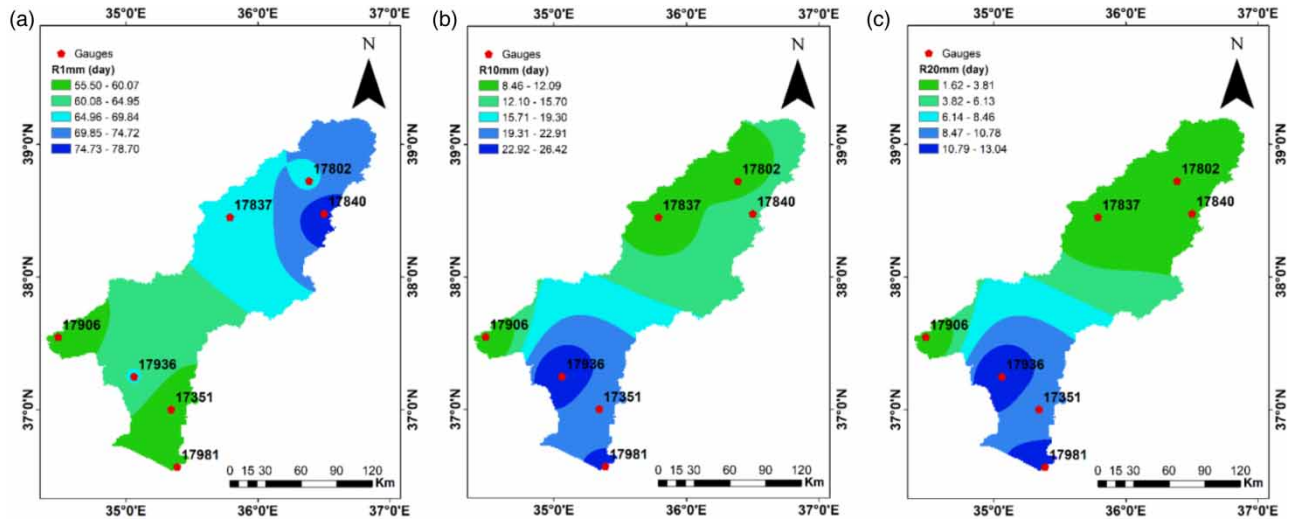

Figure 11 | Spatial variability of (a) R1mm, (b) R10mm and (c) R20mm for the whole period (1970–2019).

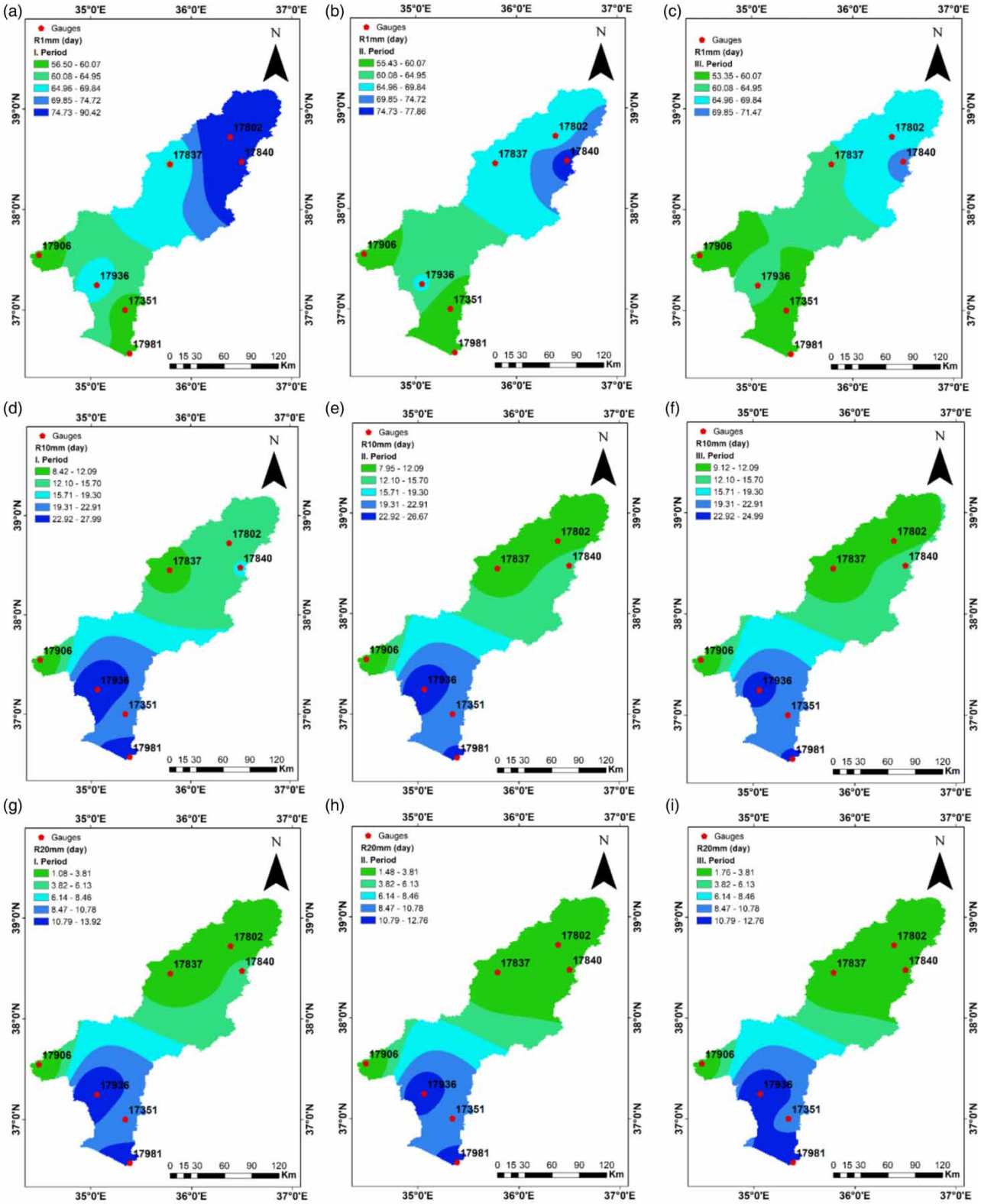

Figure 12 | Spatial variability of R1mm, R10mm and R20mm for sub-periods (a) R1mm-Period 1, (b) R1mm-Period 2, (c) R1mm-Period 3, (d) R10mm-Period 1, (e) R10mm-Period 2, (f) R10mm-Period 3, (g) R20mm-Period 1, (h) R20mm-Period 2, (i) R20mm-Period 3.

11(c)), contrary to the R1mm index, the north of the basin has low R10mm and R20mm indices, while the south has high R10mm and R20mm indices. This situation shows that heavy rains occur significantly in the south of the basin. The R10mm and R20mm indices show very similar behavior throughout the basin for the entire period. Stations 17936 and 17981 have high values in both the R10mm and R20mm indices.

When the R1mm maps for the sub-periods (Figure 12(a)–12(c)) are examined, there is a decrease in the R1mm index in the whole basin from the first period to the third period, and the wet day intervals are 33.92 days, 22.43 days and 18.12 days, respectively, in the sub-periods. The most significant decreases occur in the second period in the north of the basin (especially station 17802). As in the whole period, the north of the basin has low values and the south has high values in the R10mm and R20mm indices in the lower periods, unlike R1mm. In the sub-periods, R10mm gradually decreases in the south of the basin. There is a decrease (7.95 days) in the second period and an increase in the third period (9.12 days) in the R10mm values where the precipitation density is low. In the southern parts where the precipitation density is high, there is a slight decrease from the first period to the third period (Figure 12(d)–12(f)). The variation range of R10mm values across the basin is 19.57 days, 18.72 days and 15.87 days for each sub-period, respectively. Stations 17936 and 17981 have high values in both R10mm and R20mm in all sub-periods. In the R20mm index, there is an increase from Period 1 to Period 3 at low R20mm values in the north of the basin (Figure 12(g)–12(i)). At high R20mm values in the south of the basin, there is a decrease in Period 2 compared with Period 1, and periods 2 and 3 remain almost the same. The variation range of R20mm values across the basin is 12.84 days in the first period, 11.28 days in the second period, and 11 days in the third period. R1mm, R10mm and R20mm values across the basin show a slight decrease in the number of precipitation days from the first period to the last period.

The spatial variation of the annual maximum one-day precipitation (RX1day), maximum consecutive five-day precipitation (RX5day) and simple precipitation intensity index (SDII) values for the whole period is shown in Figure 13. The spatial distribution of all three index values in the basin is similar, and low values are found in the north of the basin and high values in the south of the basin, as in the annual mean precipitation (Figure 4(a)). Station 17936 has the highest values of the basin for all three indices. This is a sign that there may be a flood risk in the area where station 17936 is located. According to the RX1day, RX5day and SDII maps in Figure 13, the highest values of these indices are determined to be approximately three times the lowest values.

The spatial distribution of the RX1day, RX5day and SDII indices for the sub-periods is given in Figure 14. In all three indices, the north of the basin has low values and the south has high values (except for station 17906). The highest values are obtained at station 17936 in all three indices. When the lowest values of the RX1day index are examined, it is seen that there is an increase from the first period to the third period (113 mm, 122 mm, 136 mm). There is an increase in the highest RX1day values from the first period (353 mm) to the seconnd period (359 mm) and a decrease from the second period to the third period (325 mm) (Figure 14(a)–14(c)). Station 17840 receives low RX1day values after the first period. The RX1day value, which decreases in the second period at station 17351 in the south of the basin, increases in the third period.

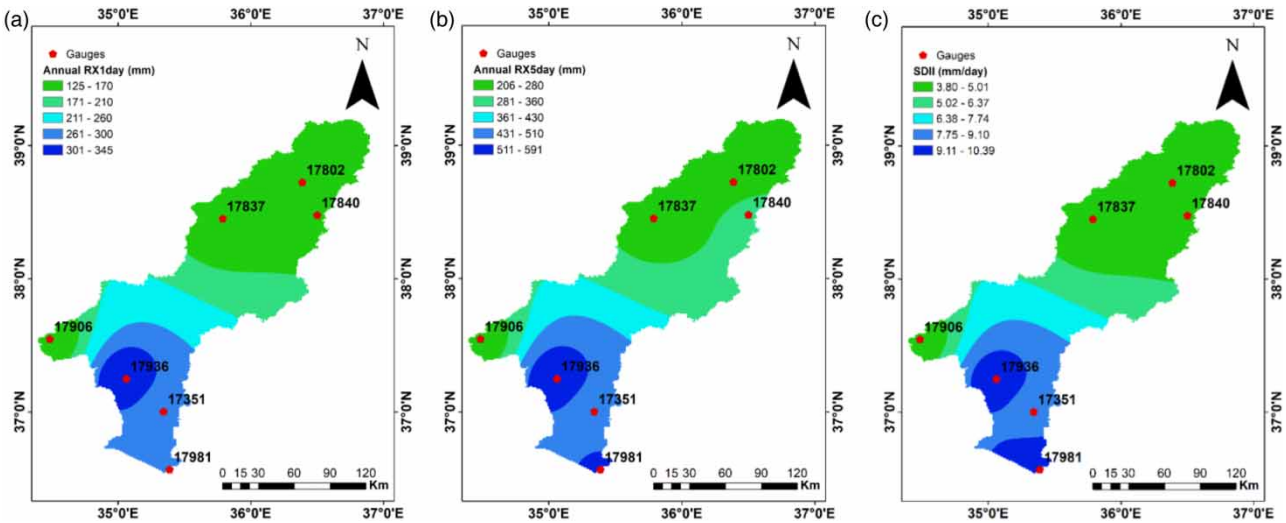

Figure 13 | Spatial variability of (a) RX1day, (b) RX5day and (c) SDII for the whole period (1970–2019).

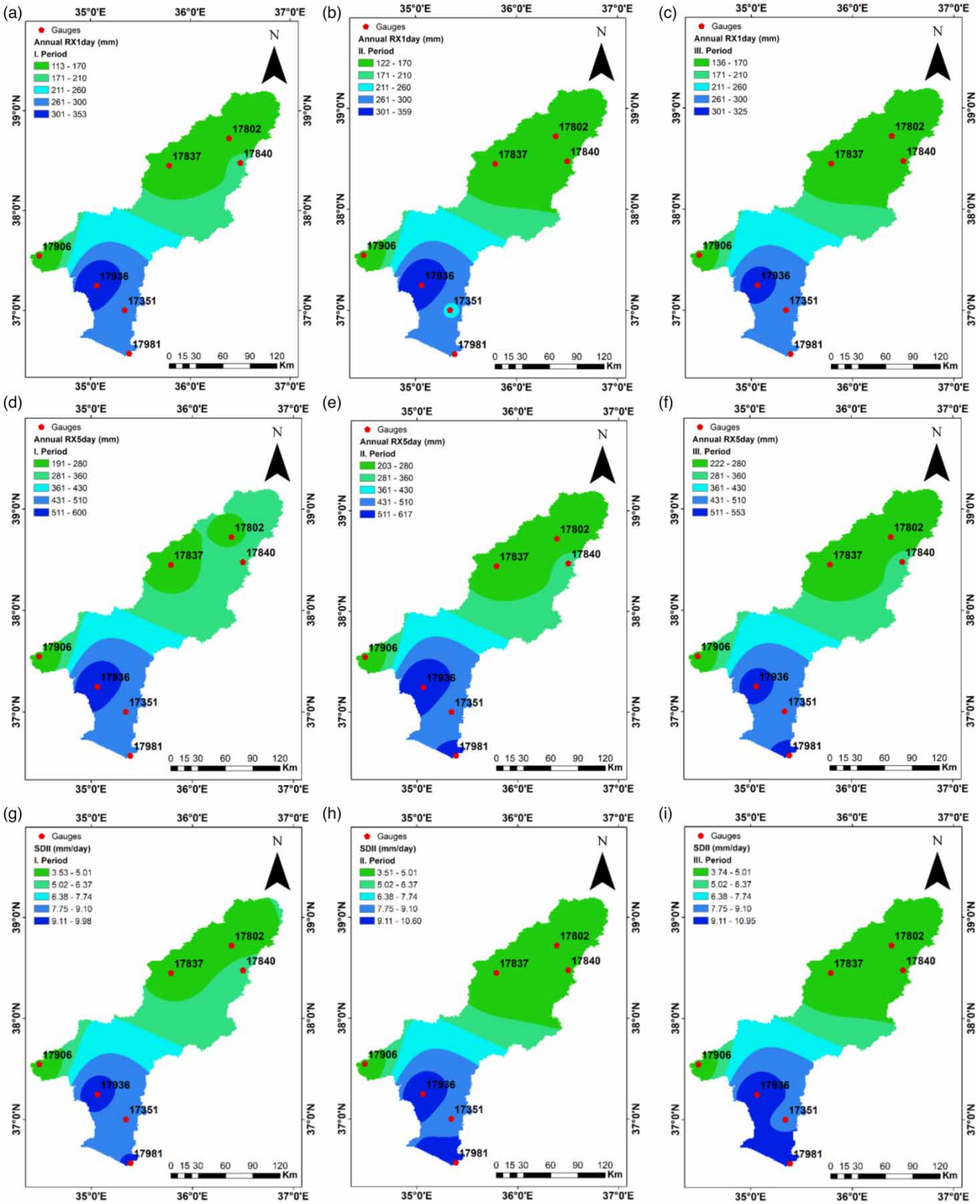

Figure 14 | Spatial variability of RX1day, RX5day and SDII mm for sub-periods: (a) RX1day-Period 1, (b) RX1day-Period 2, (c) RX1day-Period 3, (d) RX5day-Period 1, (e) RX5day-Period 2, (f) RX5day-Period 3, (g) SDII-Period 1, (h) SDII-Period 2, (i) SDII-Period 3.

According to the spatial variation of the RX5day index for the sub-periods (Figure 14(d)–14(f)), the values in the northern region of the basin increased from the first period to the third period (191 mm, 203 mm, 222 mm). The larger RX5day values in the southern part of the basin increased from Period 1 (600 mm) to Period 2 (617 mm) and decreased from Period 2 to Period 3 (553 mm), while the value of RX5day at station 17981 increased from the first period to the third period, and at station 17936 it increased a little in Period 2 and decreased again in the third period.

When the spatial variation of the SDII index for the sub-periods is examined, low SDII values are dominant in the north of the basin, and high SDII values in the south, as in RX1day and RX5day (Figure 14(g)–14(i)). The most obvious changes are seen at stations 17840, 17936 and 17981, albeit slightly. Other stations almost preserve their SDII values in all three periods. There is a slight decrease in the SDII value of station 17840 in the second period compared with the first period. At stations 17936 and 17981 in the north of the basin, an increase is observed in SDII values from the first period to the third period (Figure 14(g)–14(i)).

5. CONCLUSION

Seyhan Basin is one of the most important basins of Turkey with its rich biodiversity and socio-economic opportunities. In this study, the spatiotemporal variability of precipitation in the Seyhan Basin was investigated with daily data from seven stations for the period 1970–2019. Pettitt, Buishand rank and standard normal homogeneity tests were used to determine the breaking points in the study period with a basin-scale approach. According to the results obtained, 1981 and 2002 were determined as the breaking years.

RX1day, RX5day, SDII, CDD, CWD, R1mm, R10mm and R20mm extreme indices were also investigated in the study as well as precipitation. Then, modified Mann–Kendall and Spearman's rho trend tests were applied to precipitation and extreme indices for all periods and three sub-periods. Significant trends were detected at stations 17837, 17840 and 17906. In the temporal analysis of precipitation, the second period (01.01.1982–31.12.2002) was determined to be a period in which a decrease was generally detected in precipitation and extreme indices.

Finally, the spatial variability of precipitation was investigated with extreme indices. While the number of rainy days decreases in the south of the basin, the intensity of precipitation increases. This situation increases the frequency of sudden heavy rains. Thus, the risk of flooding is increasingly coming to the fore. Looking at the north of the basin, a general decrease in precipitation and an increase in dry days were observed. It is thought that this situation will adversely affect agricultural activities.

The potential for short-term sudden rains to occur is increasing throughout the basin. In this case, a sensitive planning study should be carried out to use water resources efficiently. A significant decrease in the number of consecutive wet days was detected in the west of the basin. Considering the general decreasing trend of precipitation, it is a negative situation in terms of water resources. When we looked at the basin in general, it was determined that the flood risk increased in the southern parts, while the drought risk came to the fore in the north.

In line with the results obtained, examining the response of the basin to precipitation variability is to be considered in future studies. By modeling the land cover and soil characteristics, important information can be obtained in understanding the rainfall–runoff relationship. Decision-makers need to develop strategies by taking into account the hydrological variability in the basin.

ACKNOWLEDGEMENTS

We would like to thank the Turkish State Meteorological Service for providing the precipitation data.

DATA AVAILABILITY STATEMENT

Data cannot be made publicly available; readers should contact the corresponding author for details.

CONFLICT OF INTEREST

The authors declare there is no conflict.

REFERENCES

Abiy, A. Z., Melesse, A. M., Abtew, W. & Whitman, D. 2019 Rainfall trend and variability in Southeast Florida: implications for fresh water availability in the Everglades. *PLoS ONE* **14** (2), e0212008. https://doi.org/10.1371/journal.pone.0212008.

Alexander, L. V., Fowler, H. J., Bador, M., Behrangi, A., Donat, M. G., Dunn, R., Funk, C., Goldie, J., Lewis, E., Rogé, M., Seneviratne, S. I. & Venugopal, V. 2019 On the use of indices to study extreme precipitation on sub-daily and daily time scales. *Environmental Research Letters* **14** (12), 125008. https://doi.org/10.1088/1748-9326/ab51b6.

Alexandersson, H. 1986 A homogeneity test applied to precipitation data. *Journal of Climatology* **6** (6), 661–675. https://doi.org/10.1002/joc.3370060607.

Altın, T. B., Sarış, F. & Altın, B. N. 2020 Determination of drought intensity in Seyhan and Ceyhan River Basins, Turkey, by hydrological drought analysis. *Theoretical and Applied Climatology* **139**, 95–107. https://doi.org/10.1007/s00704-019-02957-y.

Barbosa, H. A. & Lakshmi Kumar, T. V. 2016 Influence of rainfall variability on the vegetation dynamics over Northeastern Brazil. *Journal of Arid Environments* **124**, 377–387. https://doi.org/10.1016/j.jaridenv.2015.08.015.

Bhatti, A. S., Wang, G., Ullah, W., Ullah, S., Hagan, D. F. T., Nooni, I. K., Lou, D. & Ullah, I. 2020 Trend in extreme precipitation indices based on long term in situ precipitation records over Pakistan. *Water* **12** (3), 797. https://doi.org/10.3390/w12030797.

Boluwade, A. 2020 Spatial-temporal assessment of satellite-based rainfall estimates in different precipitation regimes in water-scarce and data-sparse regions. *Atmosphere* **11**, 901. https://doi.org/10.3390/atmos11090901.

Buishand, T. A. 1982 Some methods for testing the homogeneity of rainfall records. *Journal of Hydrology* **58** (1–2), 11–27. https://doi.org/10.1016/0022-1694(82)90066-X.

Cavus, Y. & Aksoy, H. 2019 Spatial drought characterization for Seyhan River Basin in the Mediterranean region of Turkey. *Water* **11** (7), 1331. https://doi.org/10.3390/w11071331.

Chen, Y., Guan, Y., Shao, G. & Zhang, D. 2016 Investigating trends in streamflow and precipitation in Huangfuchuan Basin with wavelet analysis and the Mann-Kendall test. *Water* **8** (3), 77. https://doi.org/10.3390/w8030077.

Elzopy, K. A., Chaturvedi, A. K., Chandran, K. M., Gopinath, G., Naveena, K. & Surendran, U. 2021 Trend analysis of long-term rainfall and temperature data for Ethiopia. *South African Geographical Journal* **103** (3), 381–394. https://doi.org/10.1080/03736245.2020.1835699.

Esmaeilpour, M., Ghasemi, A. R., Khoramabadi, F. & Rashedi, S. 2021 Spatiotemporal variability of trend in extreme precipitations using fuzzy clustering over Northwest Iran. *Earth Science Informatics* **14**, 2123–2132. https://doi.org/10.1007/s12145-021-00680-9.

Fisher, N. I., Lewis, T. & Embleton, B. J. J. 1987 *Statistical Analysis of Spherical Data*. Cambridge University Press, Cambridge, UK.

Gao, T. & Shi, X. 2016 Spatio-temporal characteristics of extreme precipitation events during 1951–2011 in Shandong, China and possible connection to the large scale atmospheric circulation. *Stochastic Environmental Research and Risk Assessment* **30** (5), 1421–1440. https://doi.org/10.1007/s00477-015-1149-7.

General Directorate of Water Management 2017 *Seyhan Basin Sectoral Water Allocation Plan*. General Directorate of Water Management, Ankara, Turkey.

Gokmen, M. 2016 Spatio-temporal trends in the hydro climate of Turkey for the last decades based on two reanalysis data sets. *Hydrology and Earth System Sciences* **20**, 3777–3788. https://doi.org/10.5194/hess-20-3777-2016.

Gumus, V. & Algin, H. M. 2017 Meteorological and hydrological drought analysis of the Seyhan–Ceyhan River Basins, Turkey. *Meteorological Applications* **24**, 62–73. https://doi.org/10.1002/met.1605.

Hamed, K. H. & Rao, A. R. 1998 A modified Mann-Kendall trend test for autocorrelated data. *Journal of Hydrology* **204**, 182–196. https://doi.org/10.1016/S0022-1694(97)00125-X.

IPCC 2021 *Climate Change 2021: The Physical Science Basis Contribution of Working Group I to the Sixth. Assessment Report of the Intergovernmental Panel on Climate Change*. Cambridge University Press, Cambridge, UK.

Jaiswal, R. K., Lohani, A. K. & Tiwari, H. L. 2015 Statistical analysis for change detection and trend assessment in climatological parameters. *Environmental Processes* **2** (4), 729–749. https://doi.org/10.1007/s40710-015-0105-3.

Jiang, P., Yu, Z., Gautam, M. R. & Acharya, K. 2016 The spatiotemporal characteristics of extreme precipitation events in the western United States. *Water Resources Management* **30**, 4807–4821. https://doi.org/10.1007/s11269-016-1454-z.

Keskiner, A. D., Cetin, M., Simsek, M., Akin, S. & Cetiner, I. 2019 Probabilistic regional meteorological drought analysis with standardized precipitation index and normal precipitation index methods in geographic information systems environment: a case study in Seyhan Basin. *Fresenius Environmental Bulletin* **28** (7), 5675–5688.

Khedhaouiria, D., Mailhot, A. & Favre, A.-C. 2020 Regional modeling of daily precipitation fields across the Great Lakes region (Canada) using the CFSR reanalysis. *Stochastic Environmental Research and Risk Assessment* **34**, 1385–1405. https://doi.org/10.1007/s00477-019-01722-x.

Lehmann, E. L. & D'Abrera, H. J. M. 1975 *Nonparametrics: Statistical Methods Based on Ranks*. Holden-Day, San Francisco, CA, USA.

Mehta, D. & Yadav, S. M. 2021 An analysis of rainfall variability and drought over Barmer District of Rajasthan, Northwest India. *Water Supply* **21** (5), 2505–2517. https://doi.org/10.2166/ws.2021.053.

Oscar-Júnior, A. C. 2021 Precipitation trends and variability in river basins in urban expansion areas. *Water Resources Management* **35**, 661–674. https://doi.org/10.1007/s11269-020-02749-4.

Pettitt, A. N. 1979 A non-parametric approach to the change-point problem. *Applied Statistics* **28** (2), 126–135. https://doi.org/10.2307/2346729.

Pour, S. H., Abd Wahab, A. K., Shahid, S. & Bin Ismail, Z. 2020 Changes in reference evapotranspiration and its driving factors in peninsular Malaysia. *Atmospheric Research* **246**, 105096. https://doi.org/10.1016/j.atmosres.2020.105096.

Ros, F. C., Tosaka, H., Sidek, L. M. & Basri, H. 2016 Homogeneity and trends in long-term rainfall data, Kelantan River Basin, Malaysia. *International Journal of River Basin Management* **14** (2), 151–163. https://doi.org/10.1080/15715124.2015.1105233.

Ryberg, K. R., Hodgkins, G. A. & Dudley, R. W. 2020 Change points in annual peak streamflows: method comparisons and historical change points in the United States. *Journal of Hydrology* **583**, 124307. https://doi.org/10.1016/j.jhydrol.2019.124307.

Rysman, J.-F., Verrier, S., Lemaître, Y. & Moreau, E. 2013 Space-time variability of the rainfall over the western Mediterranean region: a statistical analysis. *Journal of Geophysical Research: Atmospheres* **118**, 8448–8459. https://doi.org/10.1002/jgrd.50656.

Saddique, N., Khaliq, A. & Bernhofer, C. 2020 Trends in temperature and precipitation extremes in historical (1961–1990) and projected (2061–2090) periods in a data scarce mountain basin, northern Pakistan. *Stochastic Environmental Research and Risk Assessment* **34**, 1441–1455. https://doi.org/10.1007/s00477-020-01829-6.

Shawul, A. A. & Chakma, S. 2020 Trend of extreme precipitation indices and analysis of long-term climate variability in the Upper Awash Basin, Ethiopia. *Theoretical and Applied Climatology* **140**, 635–652. https://doi.org/10.1007/s00704-020-03112-8.

Sillmann, J., Kharin, V. V., Zhang, X., Zwiers, F. W. & Bronaugh, D. 2013 Climate extremes indices in the CMIP5 multimodel ensemble: part 1. Model evaluation in the present climate. *Journal of Geophysical Research: Atmospheres* **118** (4), 1716–1733. https://doi.org/10.1002/jgrd.50203.

Sneyers, R. 1990 *On the Statistical Analysis of Series of Observations.* WMO Technical Note 143, WMO No. 415, World Meteorological Organization, Geneva, Switzerland.

Talu, N. & Özüt, H. 2011 *Strategic Steps to Adapt to Climate Change in Seyhan River Basin*. Ministry of Environment and Urbanization, General Directorate of Environmental Management, Department of Climate Change, Ankara, Turkey.

Tao, Y., Wang, W., Song, S. & Ma, J. 2018 Spatial and temporal variations of precipitation extremes and seasonality over China from 1961–2013. *Water* **10** (6), 719. https://doi.org/10.3390/w10060719.

Tongal, H. 2019 Spatiotemporal analysis of precipitation and extreme indices in the Antalya Basin, Turkey. *Theoretical and Applied Climatology* **138**, 1735–1754. https://doi.org/10.1007/s00704-019-02927-4.

Topçu, E. & Seçkin, N. 2016 Drought analysis of the Seyhan Basin by using standardized precipitation index SPI and L-moments. *Journal of Agricultural Sciences* **22**, 196–215. https://doi.org/10.1501/Tarimbil_0000001381.

Tosunoğlu, F. 2017 Trend analysis of daily maximum rainfall series in Çoruh Basin, Turkey. *Igdir University Journal of the Institute of Science and Technology* **7** (1), 195–205. https://doi.org/10.21597/jist.2017127432.

Tuncok, I. K. 2016 Drought planning and management: experience in the Seyhan River Basin, Turkey. *Water Policy* **18** (S2), 177–209. https://doi.org/10.2166/wp.2016.019.

van der Pol, T. D., van Ierland, E. C., Gabbert, S., Weikard, H.-P. & Hendrix, E. M. T. 2015 Impacts of rainfall variability and expected rainfall changes on cost-effective adaptation of water systems to climate change. *Journal of Environmental Management* **154**, 40–47. https://doi.org/10.1016/j.jenvman.2015.02.016.

Wijngaard, J. B., Klein Tank, A. M. G. & Können, G. P. 2003 Homogeneity of 20th century European daily temperature and precipitation series. *International Journal of Climatology* **23** (6), 679–692. https://doi.org/10.1002/joc.906.

Zhai, J., Mondal, S. K., Fischer, T., Wang, Y., Su, B., Huang, J., Tao, H., Wang, G., Ullah, W. & Uddin, M. J. 2020 Future drought characteristics through a multi-model ensemble from CMIP6 over South Asia. *Atmospheric Research* **246**, 105111. https://doi.org/10.1016/j.atmosres.2020.105111.

Zhang, X., Alexander, L., Hegerl, G. C., Jones, P., Tank, A. K., Peterson, T. C., Trewin, B., Zwiers, F. W. 2011 Indices for monitoring changes in extremes based on daily temperature and precipitation data. *WIREs Climate Change* **2**, 851–870. https://doi.org/10.1002/wcc.147.

First received 14 July 2022; accepted in revised form 3 November 2022. Available online 14 November 2022